A Mathematical Model of a Commercial Fuel Cell for Evaluating Efficiency Under Varying Ambient Conditions

B. B. Ndebele, P. Naidoo, P. Ragimana, and M. Makhubo
Council for Scientific and Industrial Research, 1 Meiring Naude, Pretoria, bndebele@csir.co.za
Council for Scientific and Industrial Research, 1 Meiring Naude, Pretoria, pnaidoo7@csir.co.za
Council for Scientific and Industrial Research, 1 Meiring Naude, Pretoria, pragimana@csir.co.za
Council for Scientific and Industrial Research, 1 Meiring Naude, Pretoria, kmakhubo@csir.co.za

Abstract: Long-endurance aviation propulsion is currently dominated by carbon-based fuels. However, due to climate change, which is largely attributed to carbon dioxide (CO_2) emissions from human activities, aviation contributes approximately 4 %, a more climate friendly fuel is sought. Hydrogen (H_2), particularly in proton exchange membrane (PEM) fuel cells, offers a promising carbon-neutral alternative. To assess its viability, a mathematical model of a commercial fuel cell was developed to evaluate efficiency under varying ambient conditions representative of Africa climates and at high-altitude scenarios. The Nernst equation – modified to include terms for activation, polarisation, and Ohmic losses – was used to model an experimentally determined polarisation curve (current against cell voltage curve). When fit to experimental data the modified Nernst equation parameters were found to be: A = 0.0356 V, I_0 = 0.0212 Amperes, R_{int} = 0.0059 Ohms, and I_{max} = 150 Amperes where A, I_0, R_{int} and I_{max} are the Tafel slope, limit current, internal resistance, and maximum limit current, respectively. The influence of pressure and temperature were determined by varying the partial pressure of oxygen and temperature in the Nernst equation resulting in an efficiency map ($\eta(P_{O_2}, T)$). The maps showed that efficiency is high for high ambient pressure and low ambient temperature. However, the influence of ambient pressure and temperature were found to be insignificant compared to the influence of power drawn.

Keywords: Fuel cells; hydrogen; global warming.

1. Introduction

It has been noted that frequent swings between strong El Niño to strong La Niña (ENSO) cycles should be anticipated soon because of changes in the Earth's climate. The 2023-2024 rainy season fell during an El Niño cycle, resulting in severe drought and, consequently, food shortages in several Southern African countries such as Botswana, Lesotho, Namibia, Malawi, Zambia and Zimbabwe. During the same time, some countries such as Madagascar, Mozambique, Malawi, and Zambia experienced severe floods. Both extremes negatively affect vulnerable members of society by facilitating the spread of diseases (in the case of floods) or malnutrition (in the case of droughts).

The current accepted theory is that these strong and frequent swings in the ENSO cycles are due to global climate change due to human activities such as using fossil fuels for energy generation; transportation; and manufacturing. In this regard, the global aviation community has committed to net zero emissions by 2050 (Markets and Markets, 2019). This goal can be achieved using various techniques, such as the use of sustainable aviation fuels (SAF), the improvement of engine efficiency, the improvement of low drag aircraft design, and the use of hydrogen propulsion systems.

Globalisation has significantly increased the movement of people and goods worldwide, increasing the use of fossil fuels for transportation. Rapid growth in the aviation industry has drastically increased greenhouse gas (GHG) emissions. The global aviation industry has doubled its carbon dioxide emissions from 0.5 to 1.0 gigatonne between 1990 and 2019 (Ritchie, 2024). When high-altitude effects such as contrails are included, the overall contribution of aviation to global warming

is estimated to be around 3.5 to 4% (Ritchie, 2024). It is predicted that if the current growth continues and no improvements or sustainability initiatives are implemented, the transport sector carbon dioxide emissions will increase by approximately 16% by 2050 (Harvard Business School Online, 2022). As the world becomes more connected, the transportation sectors environmental footprint will drastically increase, making it imperative to implement sustainable alternatives that reduce the emissions produced.

Approximately 81% of global primary energy supply comes from fossil fuels (Abdelkareem et al., 2021). Burning coal, oil and gas in engines or power plants produces large amounts of carbon dioxide, which is a GHG, which traps the heat in the atmosphere. The transportation sector, which is dominated by internal combustion engines contributes approximately 25% of global carbon dioxide emissions (Abdelkareem et al., 2021). These emissions from cars, trucks, ships and planes are a major driver of climate change. conventional fuel combustion releases a host of pollutants that degrade air quality and ecosystems. Vehicle and jet engines emit nitrogen oxides (NO_x) and sulphur oxides (SO_x), which lead to smog and acid rain, as well as particulate matter (soot) and volatile organic compounds, which harm human health (Abdelkareem et al., 2021). For example, NO_x from aircraft and automobiles contributes to ground level ozone and respiratory problems, while SO_x and particulate emissions can cause acidification of soils and water and cardiovascular illnesses (Abdelkareem et al., 2021). Internal combustion engines in the transport sector are recognised as one of the largest contributors to these environmental issues. The continued use of conventional fossil fuels in an increasingly globalised world is fuelling climate change and environmental degradation, from rising GHG concentrations to polluted air and damaged ecosystems.

Fuel cells, specifically proton exchange membrane (PEM) fuel cells, are viewed as an alternative to combustion engines for transportation and other applications. A PEM fuel cell generates electricity through an electrochemical reaction between hydrogen gas and oxygen from air, with the by-products of this reaction being water vapour and heat, contrasting the combustion engine which releases carbon dioxide, other exhaust gases, and heat into the atmosphere. Fuel cells operate with higher efficiency than internal combustion engines (Abdelkareem et al., 2021). Hydrogen fuel cell electric vehicles (FCEVs), for example, reach around 40–60% efficiency, approximately double the efficiency of gasoline internal combustion vehicles (which are on the order of 20–30%) (Durkin et al., 2024). Abdelkareem et al. (2021) highlight that benefits of fuel cell systems include lower greenhouse gas emissions and lower fuel consumption, due to the higher efficiency compared to conventional systems.

This paper focuses on hydrogen fuel cells, with a specific focus on proton exchange membrane fuel cells. A thermodynamic model of a PEM fuel cell was sought to evaluate their behaviour in high-altitude aircrafts, as may be the use-case in disaster monitoring or long-endurance flight. The Intelligent Energy fuel cell was used as a basis for the model. Before use in flight, it was necessary to evaluate the effect of ambient pressure and temperature on the efficiency of the fuel cell. A mathematical model of a fuel cell based on available data (Intelligent Energy polarisation curve, and its cooling air flow rates) was created using Simulink® (MATLAB R2024b) (The MathWorks Inc, 2024).

2. Methodology

A proton exchange membrane fuel cell (PEMFC) is composed of two electrodes (the anode and cathode) with a proton exchange membrane (PEM) sandwiched between the two electrodes (Figure 1). The PEM allows the selective transport of protons, while electrons are conducted through an

external circuit supplying electrical energy to a connected load. The PEM is doped with platinum, which acts as a catalyst for the anodic reaction (Equation 1).

There are several ways of supplying hydrogen to the fuel cell, such as through metal hydrides, reformates, cryogenic forms, or compressed forms (Cheng et al., 2024). Oxygen can be supplied in compressed form or extracted from ambient air. In some commercially available fuel cells, oxygen is supplied from ambient air and hydrogen must be supplied from cylinders at purities exceeding 99.95% (Intelligent Energy, 2024; Mus et al, 2024). Because fuel cells also generate substantial amounts of heat, air also serves as a coolant to maintain optimal operating conditions.

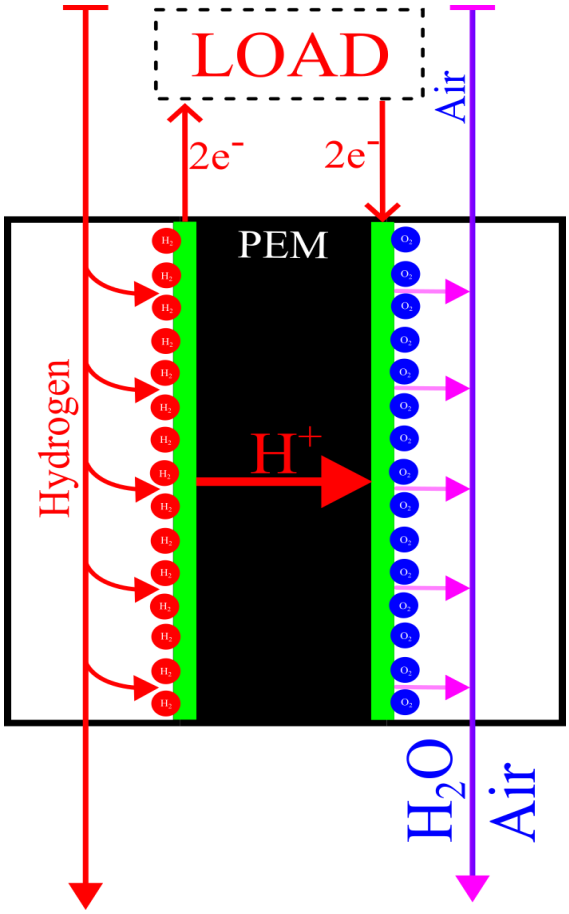

Figure 1: A schematic of a typical fuel cell.

The half-reactions shown in Equations 1 and 2 occur on the anode and cathode, respectively, to generate electrical energy, water, and heat. Three energy-loss mechanisms must be accounted for: activation losses, Ohmic losses, and concentration losses. Activation losses are related to the energy required to get the anodic and cathodic half reactions started; Ohmic losses are due to the internal resistance of the fuel cell, attributed to the movement of protons through the PEM and electrons in the external circuit; and concentration losses are due to mass transport limitations. When these losses are considered, the output voltage of a fuel cell can be modelled as Equation 3, a modified form of Nernst's equation (Datta et al, 2021). In Equation 3, the first bracketed term represents deviations from the ideal cell voltage; the second term represents activation losses; the third term represents Ohmic losses; and the last term represents concentration losses. P_i represents the partial pressure of species i; I_0 represents the exchange current; A is the Tafel slope; I_{max} represents the maximum current that can be drawn from the fuel cell; and E_0 is the cell voltage at standard conditions. R, F, n

are the molar gas constant, Faraday's constant, and the number of electrons transferred. E_{FC} and I_{FC} are the voltage and current across and through the fuel cell respectively.

$$H_2 \rightarrow 2H^+ + 2e^- \tag{1}$$

$$\frac{1}{2}O_2 + 2H^+ + 2e^- \rightarrow H_2O \tag{2}$$

$$E_{\mathrm{FC}} = E^0 + \frac{RT}{nF}\ln\left(\frac{P_{\mathrm{H_2}}{P^{0.5}}_{\mathrm{O_2}}}{P_{\mathrm{H_2O}}}\right) - A\ln\left(\frac{I_{\mathrm{FC}}}{I_0}\right) - IR_{\mathrm{int}} - \frac{RT}{nF}\ln\left(1 - \frac{I_{\mathrm{FC}}}{I_{\mathrm{max}}}\right) \tag{3}$$

It is possible to calculate the maximum possible efficiency of a fuel cell by considering the Gibbs free energy of reactions in Equations 1 and 2 and the total enthalpy when hydrogen is irreversibly oxidised. The Gibbs free energy (Equation 4) represents the useful energy that can be extracted as work from the reactions in Equations 1 and 2 by accounting for losses due to entropy (S) (Ball and Key, 2014). The efficiency of the fuel cell can then be written as Equation 5 if the electrochemical reaction occurs at a constant temperature. Table 1 shows the standard enthalpies and Gibbs free energies of formation for the reactants and products of Equations 1 and 2. From Table 1 it follows that the maximum efficiency from an ideal fuel cell is either 83% or 95% depending on whether the product (H_2O) is in liquid or vapor form, respectively. The fuel cells considered in this study form water in liquid form. Outside standard conditions, the fuel cell efficiency is therefore given by Equation 6 (where η_0 and E^0 are the efficiency and cell voltage at standard conditions) (Pilatowsky et al., 2011).

$$G = H - TS \tag{4}$$

$$\eta = \frac{\Delta G}{\Delta H} = -\frac{nFE}{\Delta H} \tag{5}$$

$$\eta = \eta_0 \frac{E_{FC}}{E^0} \tag{6}$$

Table 1: Standard enthalpies and Gibbs free energies of formation (Ball and Key, 2014)

Component	**H^0 (kJ/mol)**	**G^0 (kJ/mol)**
H^+	0	0
H_2	0	0
H_2O(g)	-241.8	-228.6
H_2O(l)	-285.8	-237.2
O_2	0	0

From Equations 3 and 6, it is obvious that the efficiency of the fuel cell is linearly dependent on temperature and logarithmically dependent on the partial pressure of oxygen (Equation 7). In Equation 7, it has been assumed that the current drawn is small ($I_{FC} \approx I_0$) so that concentration, ohmic, and activation losses can be ignored. Whether the efficiency increases or decreases with temperature is also influenced by the pressure of the reactants; however, its influence on efficiency is small relative to the influence of pressure. From Equation 7, efficiency decreases by 0.005%/K for $P_{H_2} = 0.9$ bar and $P_{O_2} = 0.21$ bar. On the other hand, efficiency increases by 2.1%/bar when $P_{O_2} = 0.21$ bar and $T = 298$ K. During flight, temperature and pressure vary simultaneously but since the influence of pressure dominates, it is expected that the efficiency of the fuel cell will decrease with increasing altitude.

$$\eta = \eta_0\left(1 + \frac{RT}{2FE^0}\ln\left(P_{\mathrm{H_2}}{P^{0.5}}_{\mathrm{O_2}}\right)\right) \tag{7}$$

Figure 2a shows a sketch of the typical voltage variation of the fuel cell with current density; the annotations show the losses that were described in Equation 3. The figure shows the trend for one cell in the fuel cell module. In a commercial fuel cell, individual cells are typically connected in series to increase the output voltage of the fuel cell module. Figure 2b shows a polarisation curve for the 1200 W Intelligent Energy fuel cell (Intelligent Energy, 2025). The figure shows the experimental curve as provided by the manufacturer superimposed on the mathematical model presented by Equation 3. The model parameters (N, A, I_0, R_{int}, and I_{max}) were estimated from the polarisation curve in Figure **2**. The number of cells were estimated as $\left\lceil \frac{E_{OC}}{1.229\ V} \right\rceil \approx 60$ with $E_{OC} \approx 71$ V where E_{OC} is the open circuit voltage. The gradient of the Ohmic region was taken to be the internal resistance. Since the manufacture's data showed the activation and Ohmic regions only, the maximum possible current (I_{max}) was set sufficiently large at 150 Amperes. With N, A, and R_{int} estimated; the Tafel slope and exchange current were found by use of the least squares deviation method to fit Equation 3 to the manufacturer's data.

Error! Reference source not found. and Figure 4 show the block diagram representing a mathematical model of a fuel cell system in MATLAB's Simscape. The fuel cell is modelled according to Equation 3 which in turn is fitted to the polarisation curve shown in **Error! Reference source not found.**b. A snippet of the code that defines the fuel cell block in **Error! Reference source not found.** is shown in **Error! Reference source not found.**. In addition to that, data from the measured fuel cell exhaust temperature was measured against power output and used to calibrate the temperature controller model, which calculates the amount of cooling air required.

The mass and energy balance equations used to model the constant volume chamber are shown in Equations 8 and 9, respectively. M, U, $\dot{m}_i$, ϕ_i and Q_H are the mass of gas in the tank, internal energy of the gas in the tank, mass flowrate into port i, bulk energy flowrate into port i, and heat flowrate through port H. The same set of equations are used to model the hydrogen tank (Figure 4). Air and hydrogen were assumed to follow Equation 10 with their respective compressibility (z). The initial gas mass, pressure, and temperature are sufficient conditions to close the system of equations 8, 9, and 10.

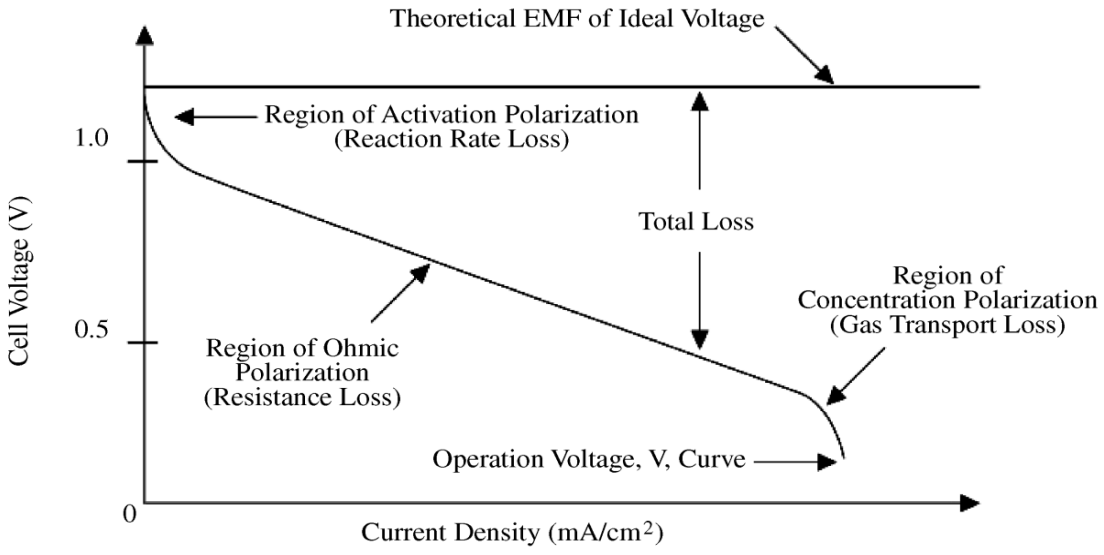

a. Characteristic cell voltage variation with current density typical for all PEMFC (EG&G Technical Services, Inc., 2004)

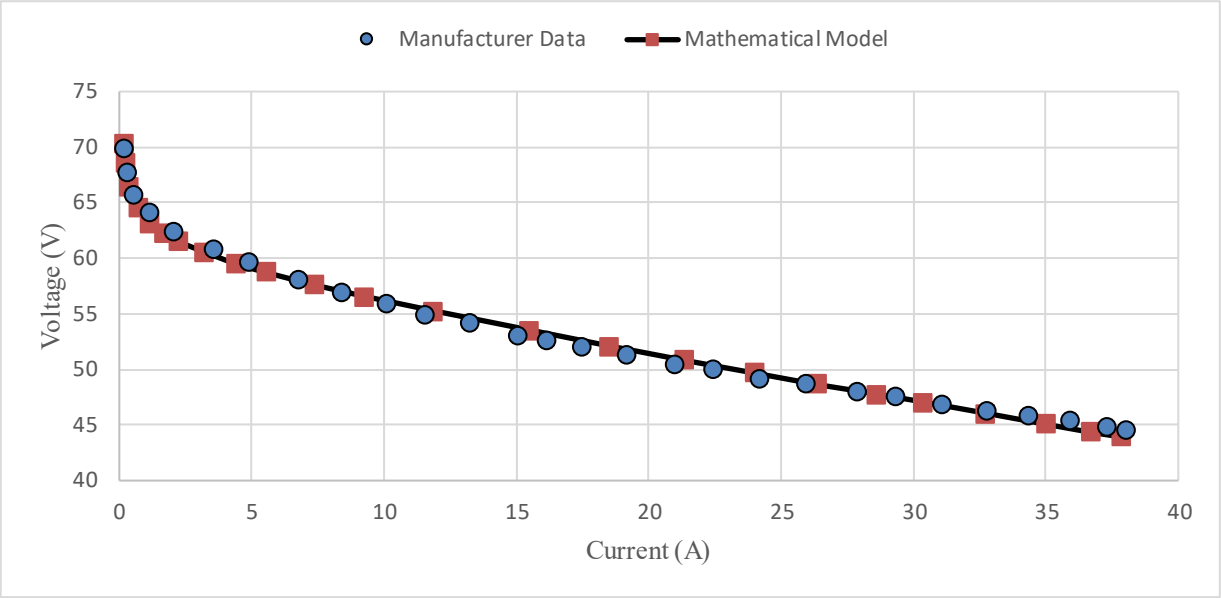

b. Polarisation curve of the Intelligent Energy 1200 W fuel cell overlayed with the mathematical model (Equation 3). In the mathematical model, $N = 60$, $A = 0.0356$ V, $I_0 = 0.0212$ Amperes, $R_{int} = 0.0059\ \Omega$, and $I_{max} = 150$ Amperes.

Figure 2: Fuel cell voltage variation with current draw. (a) shows the typical variation of all fuel cells while (b) shows that specific to the Intelligent Energy fuel cell with aggregated data for all cells.

With the fuel cell modelled as described and the generated polarisation curve matching the manufacturer's experimental data (**Error! Reference source not found.**b), the model was considered good enough and used to explore the influence of pressure and temperature on the efficiency of the fuel cell.

$$\frac{\partial M}{\partial P}\frac{dP}{dt} + \frac{\partial M}{\partial T}\frac{dT}{dt} = \dot{m}_A + \dot{m}_B \tag{8}$$

$$\frac{\partial U}{\partial P}\frac{dP}{dt} + \frac{\partial U}{\partial T}\frac{dU}{dT} = \phi_A + \phi_B + Q_H \tag{9}$$

$$P = zRT \tag{10}$$

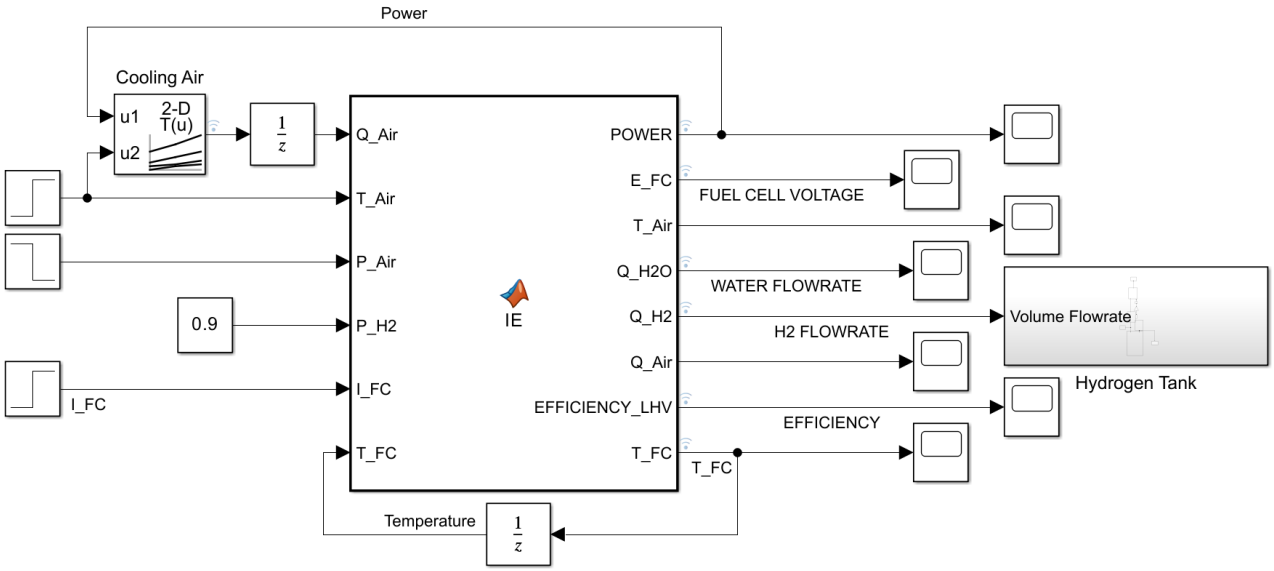

Figure 3: A mathematical model for PEMFC created using MATLAB's Simulink and Simscape.

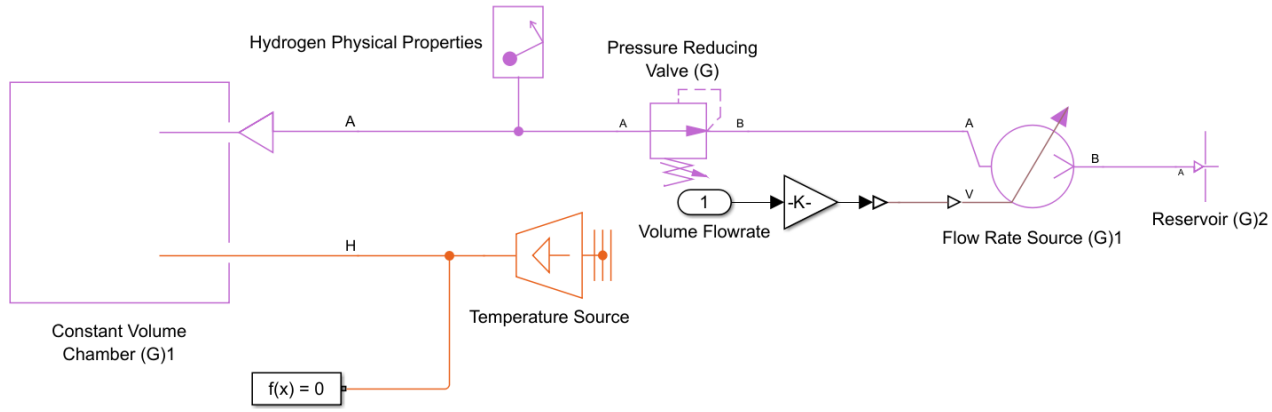

Figure 4: A block diagram of the hydrogen storage system modelled with MATLAB's Simscape.

Table 2: A snippet of the MATLAB code that models the 1200 W Intelligent Energy fuel cell

```
function [POWER, E_FC, T_Air, Q_H2O, Q_H2, Q_Air, EFFICIENCY_LHV, T_FC] = IE(Q_Air,T_Air,P_Air, P_H2, I_FC, T_FC)
%{
   P_i should be in bars and Q_i should be in L/min
%}
% Define constants
N_CELLS = 60;
TAFEL_SLOPE = 0.0356; % Volts
EXCHANGE_CURRENT = 0.0212; % Amperes
MAX_CURRENT = 150; % Amperes
INTERNAL_RESISTANCE = 0.0059; % Ohms
ENERGY_DENSITY_H2 = 120; % MJ/kg
THERMAL_MASS = 0.01; % kg
HEAT_CAPACITY_AIR = 1.005; % kJ/kg.K
TIME_STEP = 0.001;

% FLUID PROPERTIES
DENSITY_AIR = P_Air * 1E5 / (287.1 * T_Air);
DENSITY_H2 = 0.038065091; % MOL/L
MOLAR_MASS_H2O = 18.02; % grams/mol
MOLAR_MASS_H2 = 2.016; % grams/mol
DENSITY_H2O = 998; % grams/l

A = 6.022e23; % AVOGADROS_NUMBER  particles/mole
F = 96485.3321; % FARADAY_CONSTANT  s A / mol
R = 8.31446262; % MOLAR_GAS_CONSTANT  m2kg s-2K-1mol-1
e = 1.60217663e-19; % Coulomb
E0 = 1.229; % Volts

% Fuel Cell Voltage
P_O2 = 0.21 * P_Air;
E_FC = E0 + R * T_FC / (2 * F) * log(P_H2 * P_O2^0.5) - TAFEL_SLOPE * log(I_FC / EXCHANGE_CURRENT)  - I_FC *
INTERNAL_RESISTANCE  - R * T_FC / (2 * F) * log(1  - I_FC / MAX_CURRENT);
E_FC = N_CELLS * E_FC;

% Current to water
MOLES_ELECTRONS = (I_FC / (A * e));  % Moles of electrons per second
MOLES_H2_CONSUMED = 0.5 * MOLES_ELECTRONS * N_CELLS; % Moles of H2 per second
…
..
.
```

3. Results and Discussion

Error! Reference source not found. to Figure **7** show the variation in efficiency with both ambient temperature and pressure. The maps are shown for the cases where the fuel cell model was generating 125 WFigure **5**, 400 W**Error! Reference source not found.**, and 1200 W, respectively**Error! Reference source not found.**. Qualitatively, the figures show that the fuel cell model predicts the highest efficiency at high pressure and low temperature and the lowest efficiency at low pressure and high temperature. This is consistent with the inferences made earlier from Equation 7 where we see that the change in efficiency with temperature is proportional to $R/2FE^0 \ln\left(P_{O_2}^{0.5} P_{H_2}\right)$ which is

negative for the Intelligent Energy fuel cell. Similarly, the change in efficiency with pressure is proportional to the reciprocal of P_{O_2} so that efficiency increases with increasing oxygen partial pressure with that increase being more pronounced at low pressure.

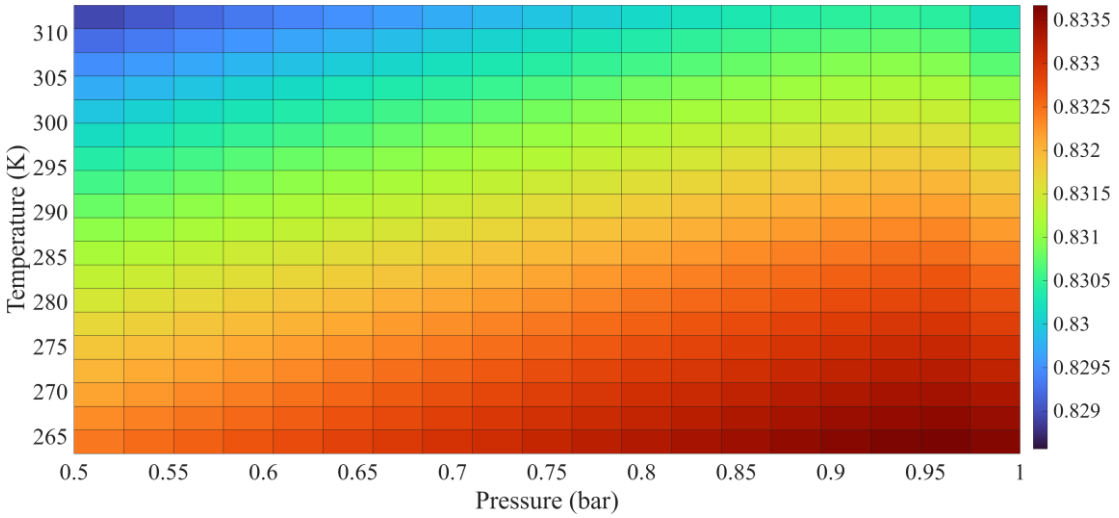

Figure 5: Efficiency map for the Intelligent Energy fuel cell as it generates 125 W.

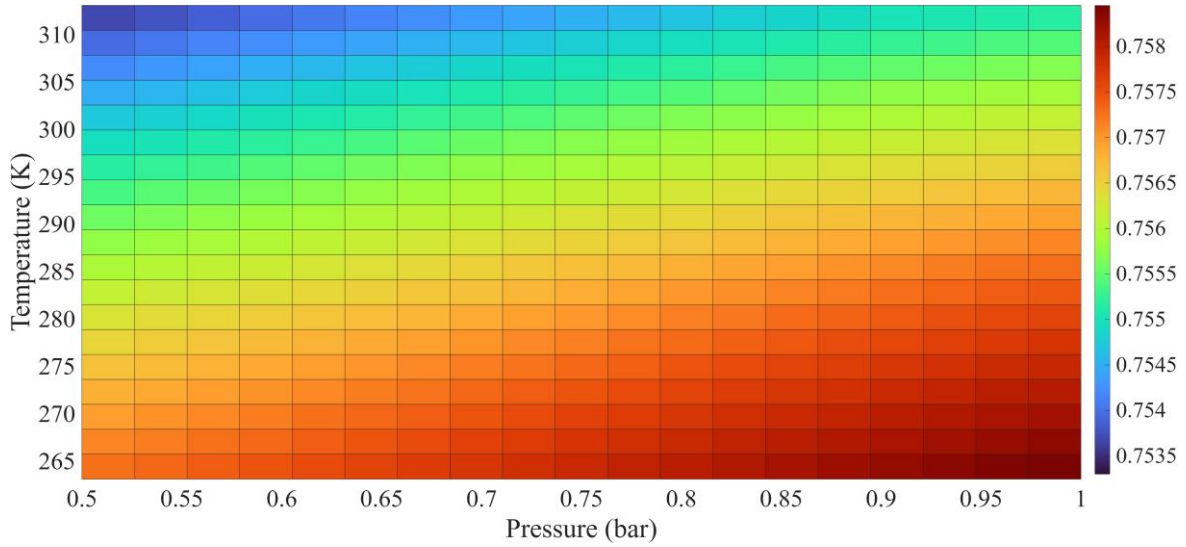

Figure 6: Efficiency map for the Intelligent Energy fuel cell as it generates 400 W.

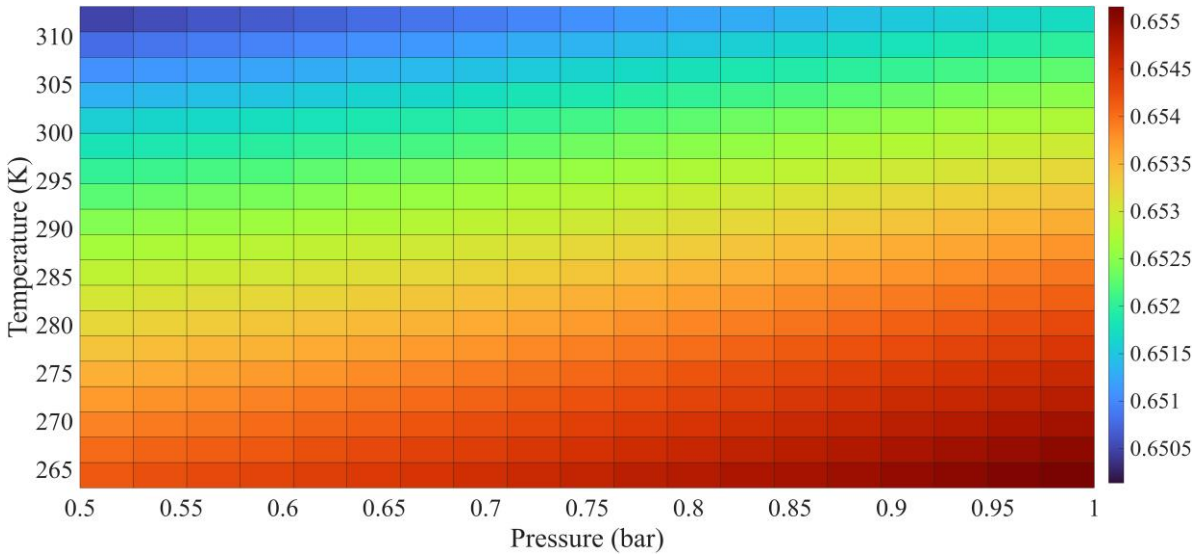

Figure 7: Efficiency map for the Intelligent Energy fuel cell as it generates 1.2 kW.

From all three plots, it appears that the effect of both temperature and pressure on efficiency is minimal. While drawing 1200 W, the efficiency range is only 0.45 % which is much smaller than the decrease in efficiency due to increasing power levels; for example, there is a 13.6 % drop in efficiency when the output power is increased from 400 W to 1200 W. It is, however, worth noting that although the oxygen partial pressure may be low there is always an excess of oxygen flowing across the fuel cell relative to the stoichiometric requirement. Additionally, while the ambient temperature may be low, the heat generated by the fuel cell is sufficient to keep the fuel cell temperature within optimal operating conditions.

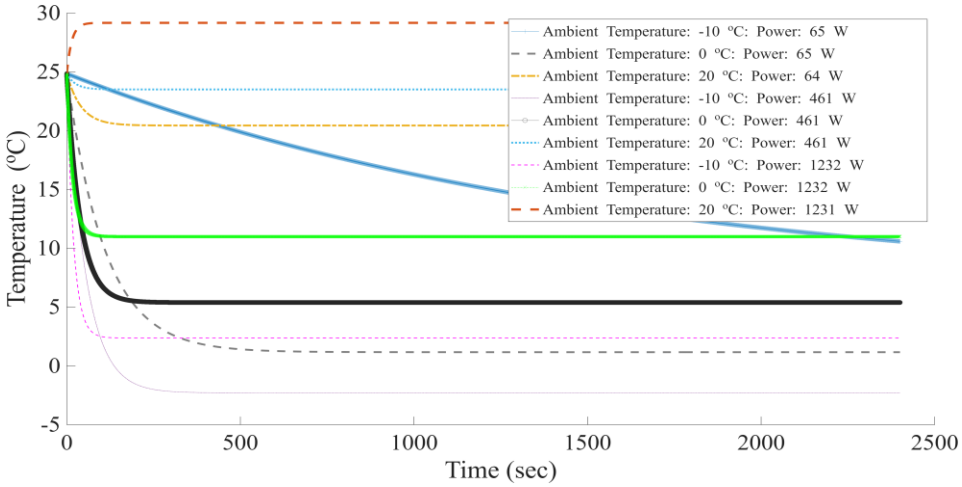

Figure 8: Variation of the fuel cell temperature with time while operating at 1 bar and different power levels.

Figure 8 shows the case for 263.15 K, 273.15 K, and 293.15 K with the fuel cell at three power levels. In nearly all cases, the steady state fuel cell temperature remains above sub-zero and within the nominal operating temperature range. The 65 W load case at a temperature of -10 °C has a subzero steady state temperature, which is not optimal since the primary by-product of the fuel cell is water which freezes at 0 °C. As such, to make sure that the fuel cell temperature remains above freezing, Intelligent Energy recommends that these commercial fuel cells be operated at at-least a third of the rated power if ambient conditions are subzero (Intelligent Energy, 2024).

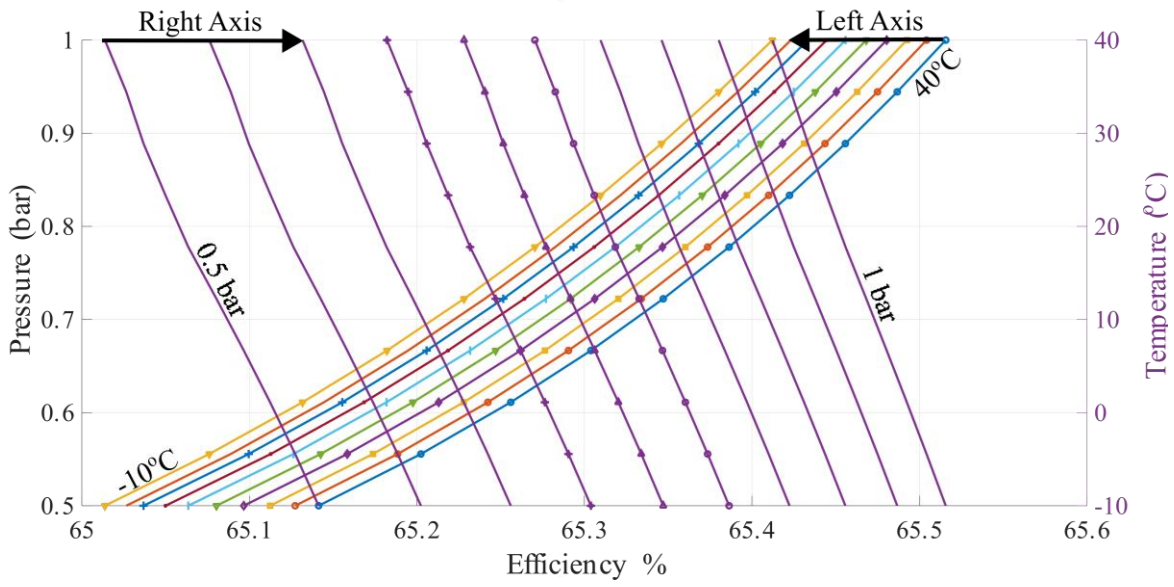

Figure 9: Efficiency variation with ambient pressure and ambient temperature

Figure **9** shows the same information as illustrated in **Error! Reference source not found.**. It shows more clearly that efficiency decreases linearly with temperature and increases logarithmically with pressure. Although Figure **9** shows the efficiency at 1.2 kW, the trend at lower power levels shows a similar pattern but scaled higher; for example, the efficiency at 400 W is generally 1.16 times that at 1.2 kW.

Since pressure and temperature vary continuously and simultaneously during flight, the variation in efficiency follows some path on the efficiency maps, such as those shown in Figs.Figure **5Error! Reference source not found.** Figure **5** to Figure **7Error! Reference source not found.**. To illustrate this variation, the flight profile in Fig.Figure **10** was investigated. Phases B to F of the flight are hover, climb to altitude, cruise, descend, and hover. In phases A and G, the aircraft is on the ground. The entire flight was assumed to take 2.8 hours. The results of this hypothetical flight are shown in Figs. Figure 11Figure **11** and Figure **12** where it can be seen that the influence of ambient temperature and pressure appears to be negligible compared to the influence of the power drawn.

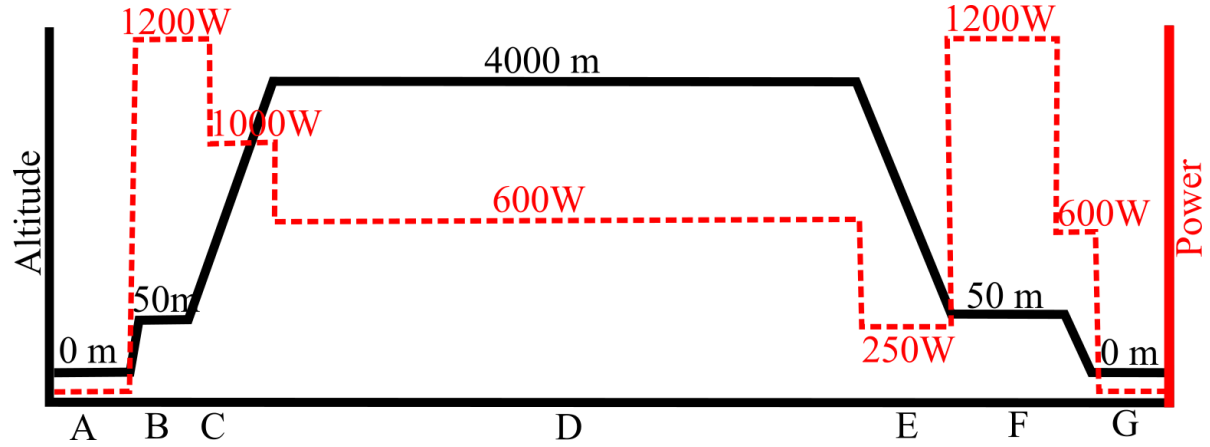

Figure 10: A typical altitude and power profile for a vertical take-off and landing aircraft.

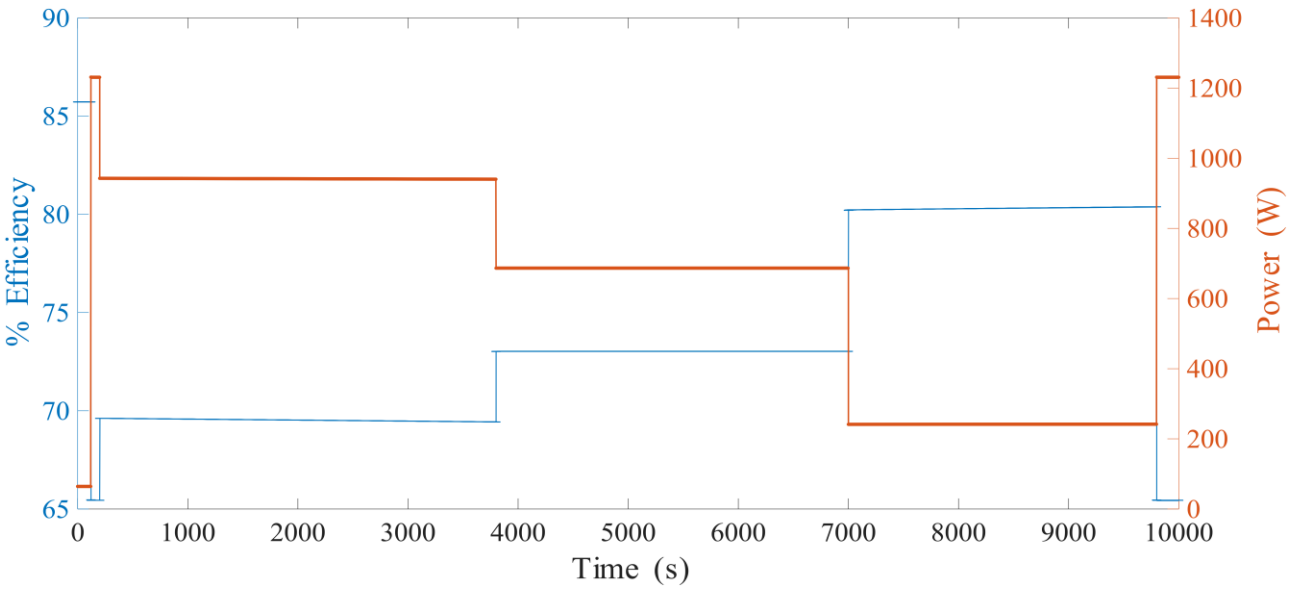

Figure 11: Efficiency over the flight profile in Fig.Figure 10.

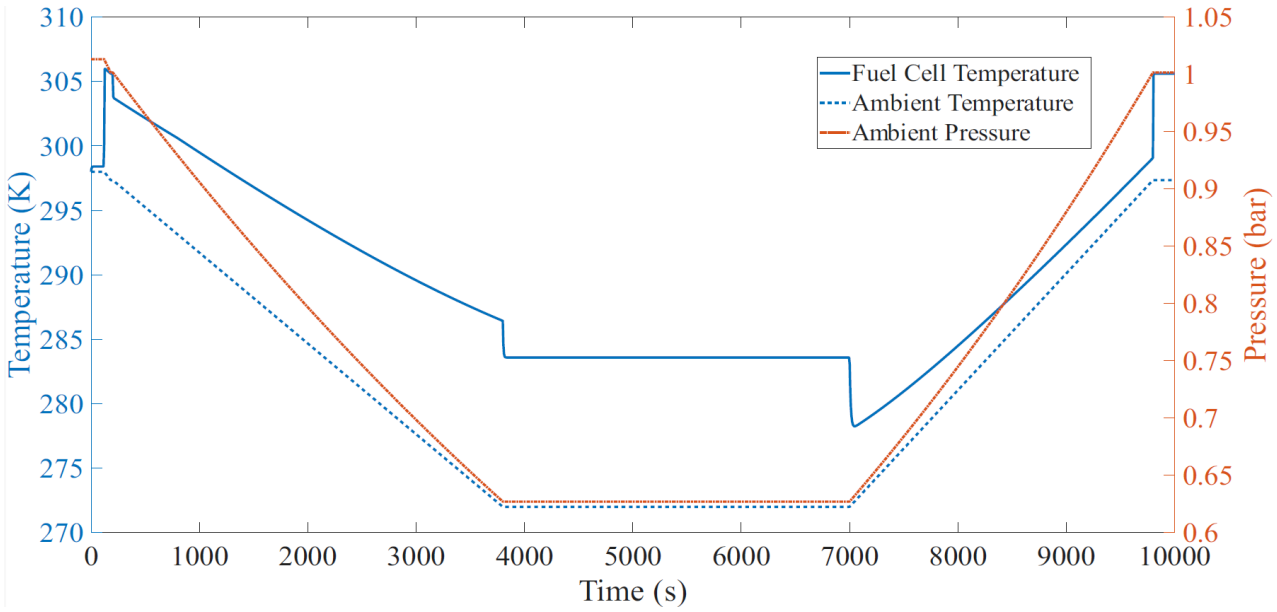

Figure 12: Ambient conditions on the flight profile in Fig.Figure 10.

4. Conclusions

From a thermodynamic perspective, it appears that the influence of ambient temperature and ambient pressure on the efficiency of a commercial fuel cell is negligible. This may be attributed to the fact that there is always an excess of air – hence oxygen – flowing across the fuel cell and excess heat that maintains the fuel cell temperature within optimal operating temperatures provided that the fuel cell is operating at at-least one third of its rated power. The mathematical model implemented in this investigation does not account for the effects of mass transport, such as the diffusion of gases and the transport of protons across the membrane, which also affect the efficiency of the fuel cell and are probably more significant. Moreover, the model does not account for parasitic losses due to cooling fans, electronics, and pumps within the system. Consequently, the actual efficiencies are lower than those calculated here.

ACKNOWLEDGEMENT(S)

This work was funded through the South African government's Parliamentary Grant.

REFERENCES CITED

1. Abdelkareem, M. A., Elsaid, K., Wilberforce, T., Kamil, M., Sayed, E. T., & Olabi, A., 2021. Environmental aspects of fuel cells: A review, Science of the Total Environment, 752, 141803. https://doi.org/10.1016/j.scitotenv.2020.141803
2. Ball, D., & Key, J. (2014). Introductory Chemistry, 1st edn. BCcampus, Victoria
3. Cheng, Q., Zhang, R., Shi, Z., & Lin, J. (2024). Review of common hydrogen storage tanks and current manufacturing methods for aluminium alloy tank liners. International Journal of Lightweight Materials and Manufacture, 7(2): 269-284
4. Datta, A., Gessow, A., & Center, R. (2021). PEM Fuel Cell model for Conceptual Design of Hydrogen eVTOL Aircraft. http://www.sti.nasa.gov
5. Durkin, K., Khanafer, A., Liseau, P., Stjernström-Eriksson, A., Svahn, A., Tobiasson, L., Andrade, T. S., & Ehnberg, J. 2024. Hydrogen-Powered Vehicles: Comparing the Powertrain Efficiency and Sustainability of Fuel Cell versus Internal Combustion Engine Cars. Energies, 17(5), 1085. https://doi.org/10.3390/en17051085

6. Harvard Business School Online. (2022, April 20). The effects of globalization on the environment. HBS Online. https://online.hbs.edu/blog/post/globalization-effects-on-environment
7. Intelligent Energy, "IE-SOAR UAV hydrogen fuel cells," Intelligent Energy; accessed 16 August, 2025, https://www.intelligent-energy.com/wp-content/uploads/2022/11/IE-SOAR-1.2kW-no-crops.pdf
8. Markets and Markets, 2019. Fixed-Wing VTOL UAV Market – Global Forecast to 2030. Accessed on 16 August 2025, https://www.marketsandmarkets.com/Market-Reports/fixed-wing-vtol-uav-market-173456250.html
9. Mus, J., Madhav, D., Vanierschot, M., Vandeginste, V., & Buysschaert, F. (2024). A review of the impact of ambient conditions and degradation in hybrid fuel cell powered unmanned aerial vehicles. In Journal of Power Sources (Vol. 624). Elsevier B.V. https://doi.org/10.1016/j.jpowsour.2024.235571
10. Pilatowsky, I., Romero, R., Isaza, C., Gamboa, S., Sebastian, P., Rivera, W. (2011). Thermodynamics of Fuel Cells. In: Cogeneration Fuel Cell-Sorption Air Conditioning Systems. Green Energy and Technology. Springer, London. https://doi.org/10.1007/978-1-84996-028-1_2
11. Ritchie, H. (2024). What share of global CO_2 emissions come from aviation? Our World in Data. https://ourworldindata.org/global-aviation-emissions
12. The MathWorks Inc. (2024). MATLAB version: 24.2.0.2740171 (R2024b), Natick, Massachusetts: The MathWorks Inc. https://www.mathworks.com